A Radiotracer for Molecular Imaging and Therapy of Gastrin-Releasing Peptide Receptor–Positive Prostate Cancer

Ivica J. Bratanovic[1], Chengcheng Zhang[1], Zhengxing Zhang[1], Hsiou-Ting Kuo[1], Nadine Colpo[1], Jutta Zeisler[1], Helen Merkens[1], Carlos Uribe[2,3], Kuo-Shyan Lin[1,2], and François Bénard[1,2]

[1]BC Cancer, Vancouver, British Columbia, Canada; [2]Department of Radiology, University of British Columbia, Vancouver, British Columbia, Canada; and [3]Functional Imaging, BC Cancer, Vancouver, British Columbia, Canada

The gastrin-releasing peptide receptor (GRPR) is overexpressed in many solid malignancies, particularly in prostate and breast cancers, among others. We synthesized ProBOMB2, a novel bombesin derivative radiolabeled with ^{68}Ga and ^{177}Lu, and evaluated its ability to target GRPR in a preclinical model of human prostate cancer. **Methods:** ProBOMB2 was synthesized in solid phase using fluorenylmethoxycarbonyl chemistry. The chelator 1,4,7,10-tetraazacyclododecane-1,4,7,10-tetraacetic acid was coupled to the *N* terminus and separated from the GRPR-targeting sequence by a cationic 4-amino-(1-carboxymethyl)-piperidine spacer. Binding affinity for both human and murine GRPR was determined using a cell-based competition assay, whereas a calcium efflux assay was used to measure the agonist and antagonist properties of the derivatives. ProBOMB2 was radiolabeled with ^{177}Lu and ^{68}Ga. SPECT and PET imaging and biodistribution studies were conducted using male immunocompromised mice bearing GRPR-positive PC-3 human prostate cancer xenografts. **Results:** Ga-ProBOMB2 and Lu-ProBOMB2 bound to PC-3 cells with an inhibition constant of 4.58 ± 0.67 and 7.29 ± 1.73 nM, respectively. ^{68}Ga-ProBOMB2 and ^{177}Lu-ProBOMB2 were radiolabeled with a radiochemical purity greater than 95%. Both radiotracers were excreted primarily via the renal pathway. PET images of PC-3 tumor xenografts were visualized with excellent contrast at 1 and 2 h after injection with ^{68}Ga-ProBOMB2, and there was very low off-target organ accumulation. ^{177}Lu-ProBOMB2 enabled clear visualization of PC-3 tumor xenografts by SPECT imaging at 1, 4, and 24 h after injection ^{177}Lu-ProBOMB2 displayed higher tumor uptake than ^{68}Ga-ProBOMB2 at 1 h after injection. ^{177}Lu-ProBOMB2 tumor uptake at 1, 4, and 24 h after injection was 14.9 ± 3.1, 4.8 ± 2.1, and 1.7 ± 0.3 percentage injected dose per gram of tissue, respectively. **Conclusion:** ^{68}Ga-ProBOMB2 and ^{177}Lu-ProBOMB2 are promising radiotracers with limited pancreas uptake, good tumor uptake, and favorable pharmacokinetics for imaging and therapy of GRPR-expressing tumors.

Key Words: gastrin-releasing peptide receptor; bombesin; prostate cancer

J Nucl Med 2022; 63:424–430
DOI: 10.2967/jnumed.120.257758

The gastrin-releasing peptide receptor (GRPR) is a transmembrane G protein–coupled receptor that is expressed in the human body's central nervous system, gastrointestinal tract, pancreas, and adrenal cortex tissues (*1*). GRPR is also aberrantly overexpressed in many solid malignancies, which include prostate, breast, lung, colon, and ovarian cancers (*2*). The overexpression of GRPR in cancer makes it an attractive target for radioligand imaging and therapy. In the past, GRPR antagonists based on bombesin (i.e., NeoBOMB1, RM2, and ProBOMB1) have been preferred over agonists because of the adverse effects observed from using the latter (*3*,*4*).

NeoBOMB1 has recently been introduced in clinical trials to image and treat GRPR-positive tumors with ^{68}Ga- and ^{177}Lu-labeled compounds, respectively (*5*). A common trend with GRPR-targeting agents in patients and preclinical animal models is the high physiologic accumulation of the radiotracer in the pancreas and gastrointestinal tract (*5*,*6*). The off-target accumulation of the radiotracer in normal organs can affect image contrast and lesion detection and limit the maximum tolerated dose of radiotracer administered for radioligand therapy (*1*). Recently, our group began to address the issue of off-target GRPR binding (i.e., in the pancreas and intestines) with the development of ProBOMB1. It contains a unique terminal LeuψPro-NH_2 sequence that significantly reduced pancreas uptake compared with NeoBOMB1 while still retaining target specificity (*7*,*8*). However, ProBOMB1 displayed lower tumor uptake with the ^{177}Lu label than did NeoBOMB1, whereas ^{68}Ga-labeled tracer uptake was similar (*7*,*8*). To improve tumor uptake and further mitigate pancreas uptake, we designed, synthesized, and evaluated ProBOMB2 (Fig. 1). ProBOMB2 contains the same GRPR-binding sequence and unique terminal LeuψPro-NH_2 as are seen in ProBOMB1 but uses a cationic 4-amino-(1-carboxymethyl)-piperidine spacer instead of a neutral *p*-aminomethylaniline-diglycolic acid spacer (Fig. 1). The cationic piperidine spacer has been used in the past with the GRPR antagonist ^{68}Ga-RM2 to improve tumor affinity and in our own lab to improve the pharmacokinetic profile of other radiotracers (*9*,*10*).

Here, we describe the synthesis and pharmacokinetic evaluation of a novel bombesin derivative, ProBOMB2. We evaluated the potential of ProBOMB2 as a theranostic agent by radiolabeling with ^{68}Ga and ^{177}Lu. Antagonistic properties were evaluated using an in vitro fluorescence-based Ca^{2+} release assay. The pharmacokinetic properties of ^{68}Ga-ProBOMB2 and ^{177}Lu-ProBOMB2 were studied in a preclinical model of human prostate cancer.

MATERIALS AND METHODS

Synthesis of ProBOMB2 and Radiolabeling

ProBOMB2 was synthesized in solid phase using a standard fluorenylmethoxycarbonyl-based approach. The synthesis of

Received Apr. 1, 2021; revision accepted Jun. 6, 2021.
For correspondence or reprints, contact Francois Benard (fbenard@bccrc.ca).
Published online Jul. 22, 2021.

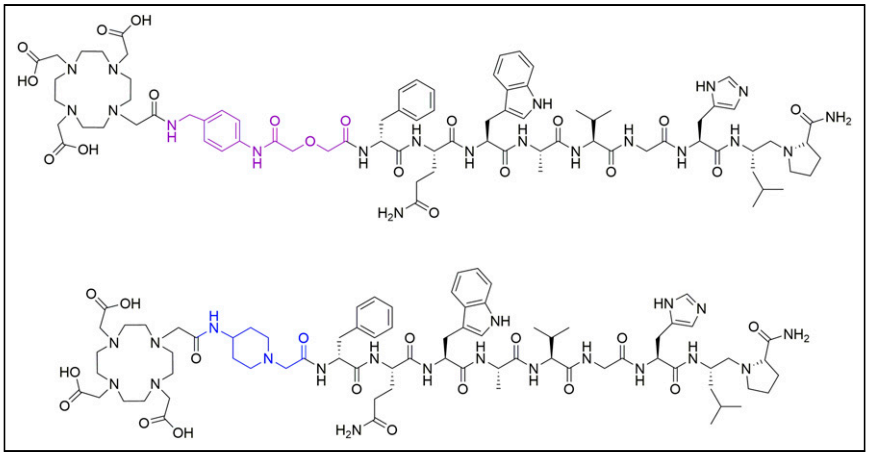

FIGURE 1. Chemical structure of ProBOMB1 (top) and ProBOMB2 (bottom)

ProBOMB2 and its lutetium and gallium cold standards is described in the supplemental materials (available at http://jnm.snmjournals.org). ProBOMB2, Ga-ProBOMB2, and Lu-ProBOMB2 were purified by high-performance liquid chromatography, and purity was confirmed by electrospray ionization mass spectrometry (supplemental materials). ProBOMB2 was radiolabeled using $^{68}GaCl_3$ to generate ^{68}Ga-ProBOMB2 and was purified using radio–high-performance liquid chromatography using the methods described in the supplemental materials. $^{177}LuCl_3$ was used to obtain ^{177}Lu-ProBOMB2, which was then purified using radio–high-performance liquid chromatography as described in the supplemental materials. The molar activity of radiotracers was measured using high-performance liquid chromatography by dividing the injected radioactivity by the tracer quantity, which was quantified by area under the ultraviolet absorbance peak and extrapolated from a standard curve. The standard curve was established with known quantities of nonradioactive Ga-ProBOMB2 or Lu-ProBOMB2.

Cell Culture

Human PC-3 prostate adenocarcinoma and murine Swiss 3T3 fibroblast cell lines were cultured and maintained in a humidified incubator (5% CO_2; 37°C) in F-12K medium and RPMI medium (Life Technologies Corp.), respectively, and supplemented with 10% fetal bovine serum, a 100 IU/mL solution of penicillin, and a 100 μg/mL solution of streptomycin (Life Technologies Corp.). PC-3 cells were chosen because of their inherent propensity to display a high surface-membrane density of human GRPR (*11*). Similarly, Swiss 3T3 cells were selected for their high surface density of murine GRPR as a way to further explain radiotracer biodistribution in our murine animal model (*12*).

Competition Binding Assay

The in vitro competition binding assays were conducted by following previously published procedures, also described in the supplemental materials (*8*).

Fluorometric Calcium Release Assay

The FLIPR Calcium 6 assay kit (Molecular Devices) was used to perform calcium release assays according to published procedures and is described in the supplemental materials (*13*).

Animal Model

Animal experiments were approved by the Animal Care Committee of the University of British Columbia. For ^{68}Ga-ProBOMB2, 8-wk-old male NOD.Cg-Prkdc^{scid}Il2rg^{tm1Wjl}/SzJ mice were obtained from an in-house colony and were inoculated subcutaneously with 5×10^6 PC-3 cells (100 μL; 1:1 phosphate-buffered saline/Matrigel; Corning), and tumors were allowed to grow for 3 wk. For ^{177}Lu-ProBOMB2, 8-wk-old male NOD.Cg-Rag1^{tm1Mom} Il2rg^{tm1Wjl}/SzJ were used instead, inoculated the same way as the NOD.Cg-Prkdc^{scid}Il2rg^{tm1Wjl}/SzJ mice.

PET/CT Imaging and Biodistribution Studies

Mice bearing PC-3 tumors were sedated (2.5% isoflurane in O_2) for intravenous injection of ^{68}Ga-ProBOMB2 (4.18 ± 0.68 MBq) and allowed to recover and roam freely in their enclosure during the uptake period. Shortly before the imaging time, the mice were sedated again under isoflurane inhalation and placed on the scanner (Inveon small-animal PET/CT scanner; Siemens Healthineers) while body temperature was maintained using a heating pad. A baseline CT scan was obtained for localization and attenuation correction (80 kV, 500 μA, and 300 ms), followed by a 10-min static PET scan at 1 or 2 h after injection of the radiotracer. After imaging, the mice were killed under isoflurane anesthesia by CO_2 inhalation, for biodistribution analysis.

The PET data were obtained in list mode, reconstructed using 3-dimensional ordered-subsets expectation maximization (2 iterations) and a maximum a priori algorithm (18 iterations) with CT-based attenuation correction. The Inveon Research Workplace software (Siemens Healthineers) was used to analyze and view the images. For biodistribution and blocking studies, the mice were injected with 1.47 ± 1.17 MBq of radiotracer. At 1 or 2 h, the mice were anesthetized with 2% isoflurane and euthanized by CO_2 inhalation. Blocking was done at 1 h via coinjection of the radiotracer with 100 μg of [D-Phe^6,Leu-NHEt^{13},des-Met^{14}]bombesin(6–14). Blood was drawn via cardiac puncture, and the organs or tissues of interest were harvested, rinsed with saline, blotted dry, weighed, and counted using an automatic γ-counter (PerkinElmer). Uptake values were expressed as percentage injected dose per gram of tissue (%ID/g).

SPECT/CT Imaging and Biodistribution Studies

PC-3 tumor–bearing mice were sedated (2.5% isoflurane in O_2), and ^{177}Lu-ProBOMB2 (34.96 ± 2.49 MBq) was administered intravenously. Before each SPECT/CT image acquisition, the mouse was given a subcutaneous injection of 250 μL of sterile saline for hydration. The same mouse was used for all imaging time-points. Mice were scanned while sedated (U-SPECT$^+$/CT; MI Labs) using an ultra-high-sensitivity big-mouse collimator (2-mm pinhole size), and body temperature was maintained using a heating pad. The CT scan was obtained using 615μA and 60kV for localization and attenuation, followed by a SPECT scan with a 20% energy window centered around 208 keV. Similarity-regulated ordered-subset expectation maximization (32 subsets, 4 iterations), a 1.0-mm postprocessing gaussian filter, and a voxel size of 0.4 mm were used to reconstruct the images. Scatter was corrected using the automatic triple energy window, and a collimator-dependent calibration factor was applied. Images were decay-corrected to the time of injection and divided by the injected activity with PMOD, version 3.402 (PMOD Technologies), to obtain quantitation in %ID/g. Data were then converted to DICOM for visualization in Inveon Research Workplace.

For biodistribution and blocking studies, the mice were injected with 2.50 ± 0.62 MBq of radiotracer. At 1, 4, 24, or 72 h, the mice were anesthetized with 2% isoflurane and euthanized by CO_2 inhalation. Blocking was done at 1 h via coinjection of the radiotracer with 100 μg of [D-Phe^6,Leu-NHEt^{13},des-Met^{14}]bombesin(6–14). Blood was drawn via cardiac puncture, and the organs or tissues of interest were collected, weighed, and counted using an automatic γ-counter (PerkinElmer). Uptake values were expressed as %ID/g.

Dosimetry

The uptake values (%ID/g) obtained from the biodistribution data were decayed to the appropriate time point and fitted to monoexponential or biexponential models using an in-house Python script (Python Software Foundation, version 3.5). Biexponential fitting assumed zero uptake at baseline. The best fit was based on the coefficient of determination (R^2) and by qualitatively looking at fits in log–log plots and their residuals. Time–activity curves were integrated to acquire residence times per unit gram and multiplied by mass of model tissue (25-g mouse whole-body phantom). The residence time data were input into OLINDA (Hermes Medical Solutions, version 2.2), which has precalculated dose factors to obtain dosimetry (*14*,*15*). Dosimetry estimations for the average adult human male were extrapolated per published procedures (*8*). Mouse biodistribution data were extrapolated to humans with the method proposed by Kirschner et al., using the following equation (*16*):

$$\left(\frac{\%\text{ID}}{m_{\text{organ}}}\right)_{\text{human}} = \left(\frac{\%\text{ID}}{m_{\text{organ}}}\right)_{\text{mouse}} \left[\frac{M_{\text{mouse}}}{M_{\text{human}}} \times (m_{\text{organ}})_{\text{human}}\right],$$

where m_{organ} is mass of organ and M represents total-body mass. Once human equivalent biodistribution values were extrapolated with the above equation, dosimetry was obtained as for the mouse case using OLINDA.

Statistical Analysis

Data were analyzed with GraphPad Prism, version 8.0. *t* tests were performed for all organs in the biodistribution studies and the binding affinity studies. For *t* tests performed for organ comparison, a correction factor was used to account for multiple comparisons using the Holm–Sidak method. The Welch *t* test was used to compare ProBOMB2 radiotracer accumulation in organs with each other and with previously established ProBOMB1 and NeoBOMB1 values. A statistically significant difference was considered present when the adjusted *P* value was less than 0.05 using the Holm–Sidak method.

RESULTS

Chemistry and Radiolabeling

The starting material fluorenylmethoxycarbonyl-LeuψPro-OH was synthesized in solution phase with 31% yield. The precursor ProBOMB2 was synthesized using fluorenylmethoxycarbonyl chemistry in solid phase. The nonradioactive Ga-ProBOMB2 and Lu-ProBOMB2 were obtained in 88% and 86% yields, respectively. Multiple batches of ^{68}Ga-ProBOMB2 were prepared in good radiochemical yield (45.5% ± 29.9%, n = 3) and good specific activity (139.86 ± 70.67 GBq/μmol, n = 3), with more than 95% radiochemical purity. ^{177}Lu-ProBOMB2 was prepared in good radiochemical yield (45.5% ± 4.4%) and high specific activity (421.8 ± 5.2 GBq/μmol), with more than 99% radiochemical purity.

Binding Affinity and Antagonist Characterization

Ga-ProBOMB2 and Lu-ProBOMB2 binding affinities were measured in human GRPR-expressing PC-3 prostate cancer cells and murine GRPR-expressing Swiss 3T3 cells (Supplemental Fig. 1; Fig. 2). The competitor ^{125}I-Tyr^{4}bombesin was successfully displaced in a dose-dependent manner by both compounds on PC-3 and Swiss 3T3 cells. Inhibition constants for Ga-ProBOMB2 and Lu-ProBOMB2 on human GRPR-expressing PC-3 cells were 4.58 ± 0.67 and 7.29 ± 1.73 nM, respectively (n = 3). Inhibition constants for Ga-ProBOMB2 and Lu-ProBOMB2 on murine GRPR-expressing Swiss 3T3 cells were 5.30 ± 1.55 and 7.91 ± 2.60 nM, respectively (n = 3). There was no significant difference in binding affinity for Ga-ProBOMB2 between murine and human GRPR (P = 0.528). Lu-ProBOMB2 also displayed no significant difference in binding affinity between murine and human GRPR (P = 0.751).

Intracellular calcium release was measured for Ga-ProBOMB2 and Lu-ProBOMB2 using PC-3 cells (Supplemental Figs. 3 and 4). Adenosine triphosphate (50 nM) and bombesin (50 nM) induced Ca^{2+} efflux corresponding to 907.3 ± 177.5 and 880.6 ± 146.3 relative fluorescence units (RFUs), compared with 6.0 ± 2.7 RFUs for buffer control. For [D-Phe^6,Leu-NHEt^{13},des-Met^{14}]bombesin(6–14) (50 nM), 5.7 ± 0.7 RFUs was observed. For Lu-ProBOMB2 (50 nM), 5.5 ± 0.8 RFUs were recorded, whereas Ga-ProBOMB2 (50 nM) elicited 6.4 ± 1.0 RFUs. Ga-ProBOMB2 RFUs were ignificantly lower from those of adenosine triphosphate (P = 0.002) and bombesin (P = 0.001) but were not significantly different from those of [D-Phe^6,Leu-NHEt^{13},des-Met^{14}]bombesin(6–14) (P = 0.299). Lu-ProBOMB2 RFUs were significantly lower than RFUs obtained with adenosine triphosphate (P = 0.002) and bombesin (P = 0.001) but were not significantly different from RFUs obtained with [D-Phe^6, Leu- NHEt^{13}, des-Met^{14}]bombesin(6–14) (P = 0.719).

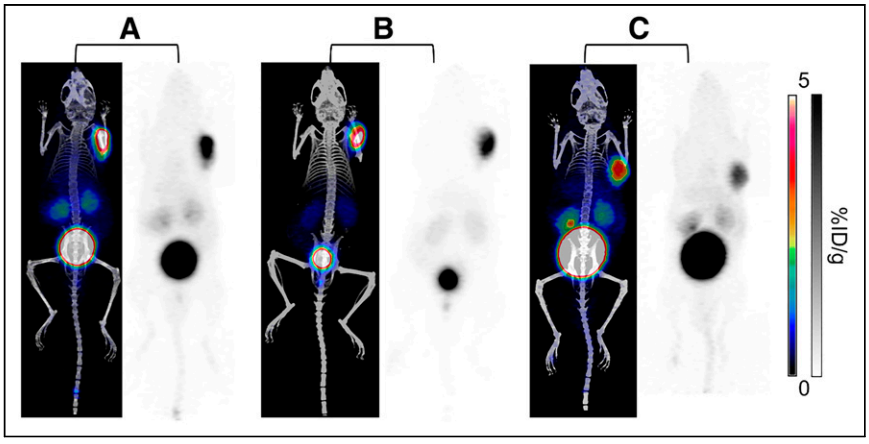

FIGURE 2. Fused maximum-intensity projection PET/CT and PET alone of ^{68}Ga-ProBOMB2 in PC-3 xenograft–bearing mice. Images were acquired at 1 h (A), 2 h (B), and 1 h with blocking (C) after injection. Blocking was performed with coinjection of 100 μg of [D-Phe^6,Leu-NHEt^{13},des-Met^{14}]bombesin(6–14).

PET Imaging and Biodistribution

The PET and PET/CT images are shown in Figure 2. There was clear visualization of PC-3 tumor xenografts in mice by ^{68}Ga-ProBOMB2, which was excreted primarily through the renal pathway. The urine contained the highest activity of ^{68}Ga-ProBOMB2, followed by the tumor and kidneys, respectively. Coinjection of the blocking agent, [D-Phe^6,Leu-NHEt^{13},des-

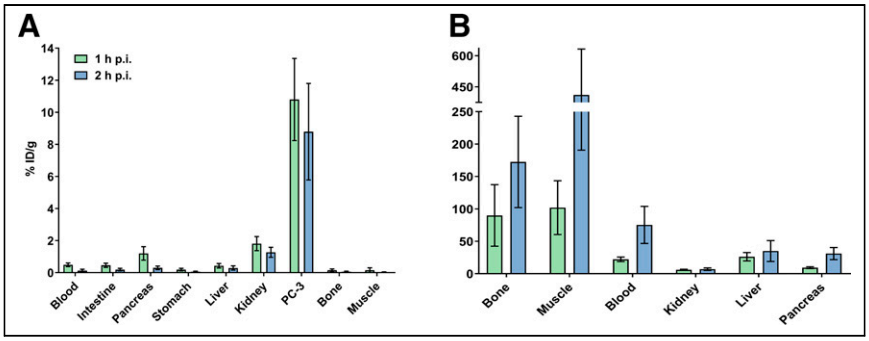

FIGURE 3. Organ uptake (A) and tumor-to-organ ratios (B) of ^{68}Ga-ProBOMB2. Time points are at 1 h and 2 h after injection in PC-3 xenograft–bearing mice. p.i. = after injection.

Met^{14}]bombesin(*6–14*), reduced tumor uptake of ^{68}Ga-ProBOMB2 by 65% at 1 h after injection. This was a significant reduction in tumor uptake compared with the unblocked sample at 1 h after injection ($P = 0.0006$).

PC-3 tumor uptake for ^{68}Ga-ProBOMB2 was 10.80 ± 2.56 and 8.79 ± 3.01 %ID/g at 1 and 2 h after injection, respectively. There was no significant difference between 1 and 2 h after injection ($P = 0.219$). Kidney uptake for ^{68}Ga-ProBOMB2 was 1.81 ± 0.44 and 1.27 ± 0.31 %ID/g at 1 and 2 h after injection, respectively. Blood, muscle, bone, and liver uptake of the PET tracer was less than 1 %ID/g across all time points (Fig. 3). Pancreas uptake was 1.20 ± 0.42 and 0.30 ± 0.11 %ID/g at 1 and 2 h after injection, respectively. Tumor-to-blood ratio increased over time from 22.19 ± 3.51 at 1 h after injection to 75.32 ± 28.59 at 2 h. Tumor-to-kidney ratios were 6.03 ± 0.88 and 6.96 ± 1.89 at 1 and 2 h after injection, respectively. Tumor-to-pancreas ratios increased from 9.32 ± 1.38 to 31.05 ± 9.28 at 1 and 2 h after injection, respectively. Tumor-to-liver ratios remained high, increasing from 26.18 ± 6.43 at 1 h after injection to 34.99 ± 16.10 at 2 h. Complete biodistribution data are presented in Supplemental Table 1.

SPECT Imaging and Biodistribution

The maximum-intensity-projection SPECT images of ^{177}Lu-ProBOMB2 are shown in Figure 4. There was clear and high-contrast visualization of PC-3 tumor xenografts in mice by ^{177}Lu-ProBOMB2 at 1, 4, and 24 h, and the tracer was then excreted renally. The highest activity for ^{177}Lu-ProBOMB2 was observed in the urine, followed by the tumor and kidneys. Coinjection of the blocking agent, [D-Phe^{6},Leu-NHEt^{13},des-Met^{14}]bombesin(6–14), decreased tumor uptake of ^{177}Lu-ProBOMB2 by 80% at 1 h after injection.

PC-3 tumor uptake for ^{177}Lu-ProBOMB2 was 14.94 ± 3.06, 4.75 ± 2.06, 1.68 ± 0.30, and 0.91 ± 0.15 %ID/g at 1, 4, 24, and 72 h after injection, respectively. Kidney uptake for ^{177}Lu-ProBOMB2 was 2.44 ± 0.59 %ID/g at 1 h after injection, which by 24 h after injection dropped to 0.71 ± 0.10 %ID/g. Pancreas uptake was 1.36 ± 0.45 %ID/g at 1 h after injection, and at 4 h after injection descended to 0.17 ± 0.06 %ID/g. Blood, muscle, bone, and liver uptake of the SPECT tracer was less than 1 %ID/g across all time points (Fig. 5). Biodistribution data for all other collected organs are presented in Supplemental Table 2. Tumor-to-blood ratio increased over time from 35.34 ± 8.47 at 1 h after injection to 320.13 ± 160.30 at 24 h. Tumor-to-kidney ratios peaked at 6.33 ± 1.60 at 1 h after injection, decreasing to 2.39 ± 0.30 at 24 h. Tumor-to-pancreas ratios increased from 11.70 ± 3.08 at 1 h after injection to 19.57 ± 4.00 at 24 h. Tumor-to-liver ratios peaked at 54.73 ± 12.31 at 1 h after injection, decreasing to 13.77 ± 4.50 at 24 h.

Dosimetry

The absorbed doses in mice injected with ^{177}Lu-ProBOMB2 are shown in Table 1. The bladder received the highest dose, followed by the PC-3 tumor and the kidneys.

Table 2 lists the estimated absorbed whole-body dose for an average adult male. These data remained consistent with the mouse model. The highest estimated normal-organ dose was in the urinary bladder, followed by the kidneys. The estimated pancreas dose remained low, along with other tissues of interest (e.g., gastrointestinal tract).

DISCUSSION

GRPR is an attractive radiopharmaceutical target for cancer therapy and diagnosis because of its overexpression in many cancer types (*1*,*17–19*). Bombesin-based GRPR antagonists can image both primary and metastatic disease in patients, particularly in estrogen receptor–positive breast cancer and prostate cancer (*5*,*6*,*8*,*20–22*). The literature largely supports the use of GRPR radiotracers for prostate cancer, for which it can be combined with prostate-specific membrane antigen radiopharmaceuticals to enhance disease management (*19*,*23*). Some bombesin-based radiotracers often accumulate in the intestine and pancreas, negatively affecting tumor contrast (*24*,*25*). Incorporating a charged hydrophilic linker in the radiotracer sequence can increase water solubility, renal excretion, and tumor uptake of radiopharmaceuticals to enhance image contrast (*26*,*27*). Novel ^{177}Lu-ProBOMB2 and ^{68}Ga-ProBOMB2 contained the unique terminal LeuψPro moiety used in ProBOMB1 but now include a cationic piperidine spacer to improve tumor uptake and contrast (*7*,*8*).

Ga-ProBOMB2 and Lu-ProBOMB2 were found to be potent GRPR antagonists, highly desirable for tolerability (*3*,*4*). ^{68}Ga-ProBOMB2 and ^{177}Lu-ProBOMB2 demonstrated high-contrast visualization of GRPR-expressing PC-3 prostate cancer xenografts

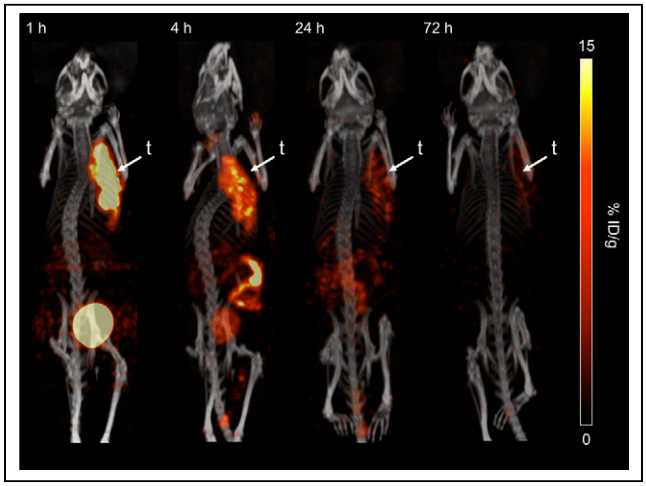

FIGURE 4. Fused maximum-intensity projection SPECT/CT of ^{177}Lu-ProBOMB2 in PC-3 xenograft–bearing mice. Acquisition time points are 1, 4, 24, and 72 h after injection. t = tumor.

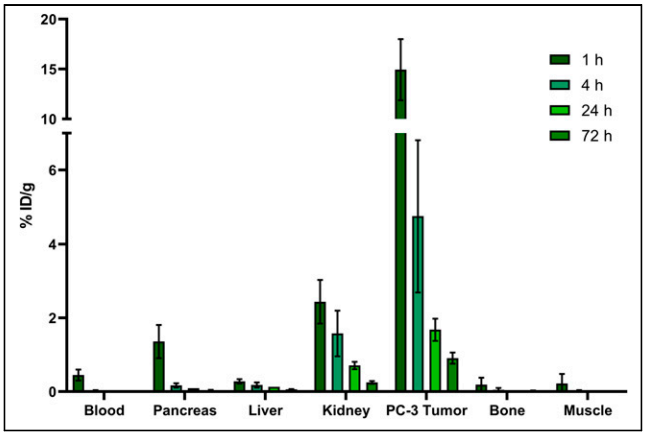

FIGURE 5. ^{177}Lu-ProBOMB2 uptake in organs of interest in PC-3–bearing mice.

with minimal normal-organ uptake on PET and SPECT imaging, respectively. Both radiotracers were rapidly excreted from the blood and peripheral organs through the renal pathway. Blocking studies confirmed radiotracer specificity for GRPR. Although blocking was not complete, decreasing tumor uptake from 10.8 %ID/g to 3.77 %ID/g, this decrease likely reflected an insufficient dose of the blocking competitor, [D-Phe6,Leu-NHEt13,des-Met14]-bombesin, or differences in the clearance profile of the competitor relative to the radioligand. Complete biodistribution studies corroborated the quality of the PET and SPECT images, indicating high, rapid normal-organ clearance of the radiotracers (Figs. 2 and 4). Tumor uptake peaked at 1 h after injection for both the ^{68}Ga and the ^{177}Lu radiotracers, each with minimal pancreas and kidney uptake. These are unique outcomes, as previous GRPR antagonists characteristically have significant pancreas and normal-organ accumulation (i.e., RM2 and NeoBOMB1) (*19*,*20*). Our ProBOMB2 radiotracers have an inherent specificity for GRPR-positive cancer tissue but not healthy tissue that expresses GRPR (i.e., the pancreas). Our binding affinity experiments showed that that the lack of pancreas and intestine uptake is not due to the interspecies difference in the GRPR structure of our animal model; rather, it is a unique property of ProBOMB2 that warrants further investigation.

TABLE 1
Absorbed Doses per Unit of Injected Activity in Mice for ^{177}Lu-ProBOMB2

Target organ	Absorbed dose (mGy/MBq)
Brain	0.99
Large intestine	2.17
Small intestine	2.09
Stomach	1.89
Heart	2.24
Kidneys	42.70
Liver	9.34
Lungs	7.50
Pancreas	8.64
Bone	6.28
Spleen	8.15
Testes	2.76
Thyroid	0.83
Bladder	632.00
Remainder of body	5.64
Tumor	134.63

TABLE 2
Estimated Organ-Absorbed Doses of ^{177}Lu-ProBOMB2 for Adult Human Male

Target organ	Absorbed dose (mGy/MBq)
Adrenals	7.51E−03
Brain	7.43E–035
Esophagus	3.18E–034
Eyes	2.57E–034
Gallbladder wall	3.91E–034
Left colon	7.57E–034
Small intestine	7.54E–034
Stomach wall	3.67E–034
Right colon	5.48E–034
Rectum	7.06E–034
Heart	7.45E–034
Kidneys	1.53E–032
Liver	3.15E–033
Lungs	2.75E–033
Pancreas	2.82E–033
Prostate	6.09E–034
Salivary glands	2.65E–034
Red marrow	3.45E–034
Skeleton	4.72E–034
Spleen	2.73E–033
Testes	6.96E–034
Thymus	2.96E–034
Thyroid	2.84E–034
Urinary bladder	5.27E–032
Remainder of body	8.03E–034

The biodistribution of ^{68}Ga-ProBOMB2, compared with that of ^{68}Ga-NeoBOMB1, found that at 1 h after injection there was a significantly lower retention of ^{68}Ga-ProBOMB2 in nontarget tissues, such as the blood, intestines, stomach, liver, pancreas, and kidneys ($P < 0.05$), while maintaining similar tumor uptake ($P > 0.05$) (Fig. 6) (*8*). The same pattern was observed when comparing ^{177}Lu-ProBOMB2 with ^{177}Lu-NeoBOMB1. The significantly higher tumor uptake for ^{177}Lu-ProBOMB2 than for ^{177}Lu-NeoBOMB1 ($P < 0.05$) at 1 h after injection is a promising characteristic, as there was significantly lower uptake of our radiotracer in the blood, intestine, pancreas, and liver ($P < 0.05$) (Fig. 6) (*7*). However, ^{177}Lu-ProBOMB2 had significant washout from the tumor at 4 h after injection, resulting in lower tumor uptake than that of ^{177}Lu-NeoBOMB1 (Fig. 6). The GRPR radiotracer profile of high pancreas uptake is also observed in RM2, a clinically established GRPR-specific radiotracer (*22*). ^{68}Ga-RM2 presented with notably high pancreas uptake in both preclinical and clinical studies (*20*,*22*). With the same prostate cancer model as in our

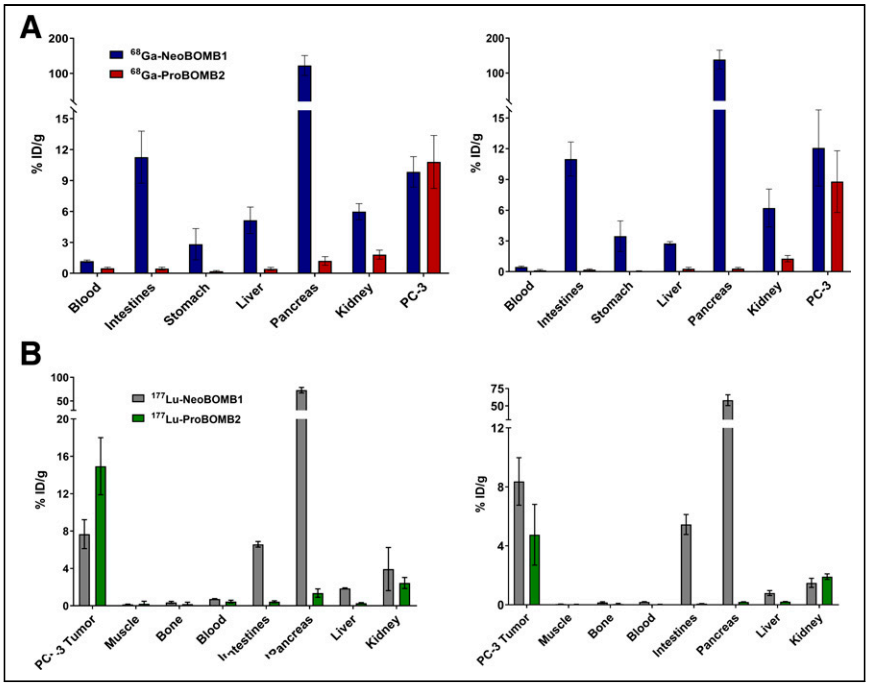

FIGURE 6. (A) Comparison of ^{68}Ga-ProBOMB2 and ^{68}Ga-NeoBOMB1 biodistributions in key organs in PC-3 tumor–bearing mice. Biodistribution data are for 1 h after injection (left) and 2 h after injection (right) (*8*). (B) Comparison of ^{177}Lu-ProBOMB2 and ^{177}Lu-NeoBOMB1 uptake in key organs in PC-3 tumor–bearing mice. Biodistribution data are for 1 h after injection (left) and 4 h after injection (right) (*7*).

study, ^{68}Ga-RM2 achieved similar tumor uptake at 1 and 2 h after injection but had higher pancreatic accumulation (*20*).

Both ^{177}Lu-ProBOMB2 and ^{68}Ga-ProBOMB2 are strong candidates for clinical translation. They demonstrated rapid clearance, resulting in high tumor-to-blood, -bone, and -muscle ratios. Importantly, a high tumor-to-pancreas ratio was obtained, with pancreas being the common dose-limiting organ for ^{177}Lu-RM2 and ^{177}Lu-NeoBOMB1 (*5*,*28*). ProBOMB2 is a GRPR antagonist, and there was washout of the radiotracer from the tumor over time. Sustained tumor uptake is desirable to enhance the radiation dose delivered to tumors relative to normal organs. Further improvements in tumor retention may be achieved by improving the metabolic stability of bombesin derivatives.

Because ProBOMB2 was excreted primarily renally, the bladder received the highest absorbed dose in our mouse model, followed by the kidneys (Table 2). This route is likely due to high blood and tumor clearance of our radiotracer. In future iterations, the radiotracer's biologic half-life can be increased using albumin binders to attenuate bladder dosing and mitigate tissue damage. The remaining organs had a low absorbed dose and were comparable to each other. When compared with published data for ^{177}Lu-labeled NeoBOMB1 and ProBOMB1, the predicted dose with ^{177}Lu-ProBOMB2 for a human adult male was much lower for many key organs (Fig. 7). The average male would be expected to receive approximately a 100 times lower dose to the pancreas with ^{177}Lu-ProBOMB2 than with ^{177}Lu-NeoBOMB1.

The favorable distribution profile of ProBOMB2 has the potential to reduce radiation exposure to normal organs and is a promising alternative for therapy of GRPR-positive cancers.

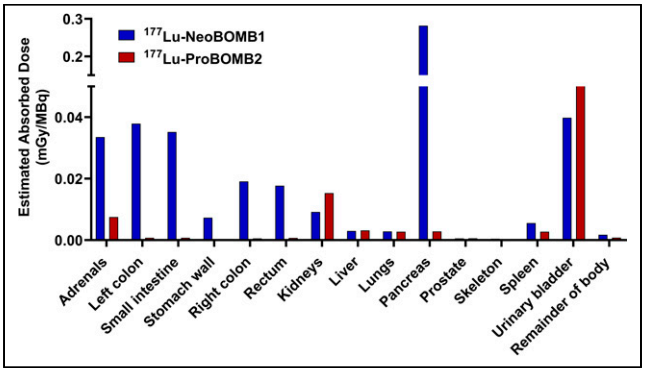

FIGURE 7. Estimated human absorbed doses of ^{177}Lu-labeled NeoBOMB1 and ProBOMB2 for average adult male (*7*).

CONCLUSION

We synthesized ProBOMB2, a GRPR-targeting peptide with nanomolar affinity for the receptor, and successfully radiolabeled it with ^{68}Ga and ^{177}Lu. ^{68}Ga- and ^{177}Lu-ProBOMB2 were able to provide high-contrast images of GRPR-expressing tumors in a preclinical human prostate cancer model with PET and SPECT, respectively, with minimal pancreas uptake. With high tumor-to-pancreas and normal-organ uptake ratios and favorable dosimetry, ^{68}Ga- and ^{177}Lu-ProBOMB2 warrant further investigation as a theranostic pair for cancer imaging and therapy.

DISCLOSURE

Francois Benard and Kuo-Shyan Lin are cofounders, directors, and shareholders of α-9 Theranostics, Inc. Chengcheng Zhang, Zhengxing Zhang, Hsiou-Ting Kuo, and Helen Merkens are shareholders of α-9 Theranostics, and Chengcheng Zhang is also a consultant. The authors of this article are coinventors on a provisional patent application related to the materials presented in this article. No other potential conflict of interest relevant to this article was reported.

KEY POINTS

QUESTION: How well does the peptide ProBOMB2 bind to GRPR and allow imaging of GRPR-positive cancers when radiolabeled with either ^{68}Ga or ^{177}Lu?

PERTINENT FINDINGS: ProBOMB2 radiolabeled with ^{68}Ga or ^{177}Lu accumulated specifically in GRPR-positive neoplastic tissue, with minimal normal-organ uptake. Uptake in the pancreas was significantly decreased, compared with previous GRPR-targeting radiopeptides (i.e., NeoBomb1), while maintaining sustained tumor uptake.

IMPLICATIONS FOR PATIENT CARE: ProBOMB2 accumulates in GRPR-positive neoplasms while having lower uptake in healthy tissues (i.e., the pancreas), thus improving image contrast for diagnostic use and reducing off-target tissue damage for therapeutic applications.

REFERENCES

1. Jensen RT, Battey JF, Spindel ER, Benya RV. International Union of Pharmacology: LXVIII—mammalian bombesin receptors: nomenclature, distribution, pharmacology, signaling, and functions in normal and disease states. *Pharmacol Rev.* 2008;60:1–42.
2. Cornelio DB, Roesler R, Schwartsmann G. Gastrin-releasing peptide receptor as a molecular target in experimental anticancer therapy. *Ann Oncol.* 2007;18:1457–1466.
3. Cescato R, Maina T, Nock B, et al. Bombesin receptor antagonists may be preferable to agonists for tumor targeting. *J Nucl Med.* 2008;49:318–326.
4. Bodei L, Ferrari M, Nunn A, et al. ^{177}Lu-AMBA bombesin analogue in hormone refractory prostate cancer patients: a phase I escalation study with single-cycle administrations [abstract]. *Eur J Nucl Med Mol Imaging.* 2007;34(suppl):S221.
5. Dalm SU, Bakker IL, De Blois E, et al. ^{68}Ga/^{177}Lu-NeoBOMB1, a novel radiolabeled GRPR antagonist for theranostic use in oncology. *J Nucl Med.* 2017;58:293–299.
6. Zang J, Mao F, Wang H, et al. ^{68}Ga-NOTA-RM26 PET/CT in the evaluation of breast cancer: a pilot prospective study. *Clin Nucl Med.* 2018;43:663–669.
7. Rousseau E, Lau J, Zhang Z, et al. Comparison of biological properties of [^{177}Lu]Lu-ProBOMB1 and [^{177}Lu]Lu-NeoBOMB1 for GRPR-targeting. *J Labelled Comp Radiopharm.* 2020;63:56–64.
8. Lau J, Rousseau E, Zhang Z, et al. Positron emission tomography imaging of the gastrin-releasing peptide receptor with a novel bombesin analogue. *ACS Omega.* 2019;4:1470–1478.
9. Zhang Z, Amouroux G, Pan J, et al. Radiolabeled B9958 derivatives for imaging bradykinin B1 receptor expression with positron emission tomography: effect of the radiolabel-chelator complex on biodistribution and tumor uptake. *Mol Pharm.* 2016;13:2823–2832.
10. Zhang C, Zhang Z, Lin KS, et al. Preclinical melanoma imaging with ^{68}Ga-labeled α-melanocyte-stimulating hormone derivatives using PET. *Theranostics.* 2017;7:805–813.
11. Reile H, Armatis PE, Schally AV. Characterization of high-affinity receptors for bombesin/gastrin releasing peptide on the human prostate cancer cell lines PC-3 and DU-145: internalization of receptor bound ^{125}I-(Tyr4) bombesin by tumor cells. *Prostate.* 1994;25:29–38.
12. Zachary I, Rozengurt E. High-affinity receptors for peptides of the bombesin family in Swiss 3T3 cells. *Proc Natl Acad Sci USA.* 1985;82:7616–7620.
13. Amouroux G, Pan J, Jenni S, et al. Imaging bradykinin B1 receptor with ^{68}Ga-labeled [des-Arg10]kallidin derivatives: effect of the linker on biodistribution and tumor uptake. *Mol Pharm.* 2015;12:2879–2888.
14. Stabin MG, Sparks RB, Crowe E. OLINDA/EXM: the second-generation personal computer software for internal dose assessment in nuclear medicine. *J Nucl Med.* 2005;46:1023–1027.
15. Keenan MA, Stabin MG, Segars WP, Fernald MJ. RADAR realistic animal model series for dose assessment. *J Nucl Med.* 2010;51:471–476.
16. Kirschner AS, Ice RD, Beierwaltes WH. Radiation dosimetry of ^{131}I 19 iodocholesterol. *J Nucl Med.* 1973;14:713–717.
17. Patel O, Shulkes A, Baldwin GS. Gastrin-releasing peptide and cancer. *Biochim Biophys Acta.* 2006;1766:23–41.
18. Nock BA, Kaloudi A, Lymperis E, et al. Theranostic perspectives in prostate cancer with the gastrin-releasing peptide receptor antagonist NeoBOMB1: preclinical and first clinical results. *J Nucl Med.* 2017;58:75–80.
19. Maina T, Nock BA, Kulkarni H, Singh A, Baum RP. Theranostic prospects of peptide receptor–radioantagonists in oncology. *PET Clin.* 2017;12:297–309.
20. Mansi R, Wang X, Forrer F, et al. Development of a potent DOTA-conjugated bombesin antagonist for targeting GRPr-positive tumours. *Eur J Nucl Med Mol Imaging.* 2011:97–107.
21. Morgat C, MacGrogan G, Brouste V, et al. Expression of gastrin-releasing peptide receptor in breast cancer and its association with pathologic, biologic, and clinical parameters: a study of 1,432 primary tumors. *J Nucl Med.* 2017;58:1401–1407.
22. Stoykow C, Erbes T, Maecke HR, et al. Gastrin-releasing peptide receptor imaging in breast cancer using the receptor antagonist ^{68}Ga-RM2 and PET. *Theranostics.* 2016;6:1641–1650.
23. Mansi R, Minamimoto R, Iagaru AH. Bombesin-targeted PET of prostate cancer. *J Nucl Med.* 2016;57(suppl):67S–72S.
24. Lin KS, Luu A, Baidoo KE, et al. A new high affinity technetium-99m-bombesin analogue with low abdominal accumulation. *Bioconjug Chem.* 2005;16:43–50.
25. Nock BA, Nikolopoulou A, Galanis A, et al. Potent bombesin-like peptides for GRP-receptor targeting of tumors with ^{99m}Tc: a preclinical study. *J Med Chem.* 2005;48:100–110.
26. Figueroa SD, Volkert WA, Hoffman TJ. Evaluation of the pharmacokinetic effects of various linking group using the ^{111}In-DOTA-X-BBN (7-14)NH2 structural paradigm in a prostate cancer model. 2009;19:1803–1812.
27. García Garayoa E, Schweinsberg C, Maes V, et al. Influence of the molecular charge on the biodistribution of bombesin analogues labeled with the [^{99m}Tc(CO)3]-core. *Bioconjug Chem.* 2008;19:2409–2416.
28. Kurth J, Krause BJ, Schwarzenböck SM, Bergner C, Hakenberg OW, Heuschkel M. First-in-human dosimetry of gastrin-releasing peptide receptor antagonist [^{177}Lu]Lu-RM2: a radiopharmaceutical for the treatment of metastatic castration-resistant prostate cancer. *Eur J Nucl Med Mol Imaging.* 2020;47:123–135.